CHAPTER 7

Insertion Electrodes for Magnesium Batteries: Intercalation and Conversion

H. D. YOO*[a] AND S. H. OH*[b]

[a]Pusan National University, Department of Chemistry, Busan 46241, Republic of Korea; [b]Korea Institute of Science and Technology, Centre for Energy Storage Research, Seoul 02792, Republic of Korea
*E-mail: hyundeog.yoo@pusan.ac.kr, sho74@kist.re.kr

7.1 Introduction

Layered materials are composed of two-dimensional (2D) layers, which are weakly bound by van der Waals forces. In contrast to 1D and 3D networks with rigid structures, weakly bound 2D networks provide structural flexibility to intercalate various kinds of ions or molecules, such as protons, alkali metal ions, amines, and organic cations. Intercalation of organic species expands the interlayer distance in a controllable manner without exfoliating the structure into single layers, signifying structural flexibility.[1–3] Likewise, intercalation of ions into layered materials undergoes topotactic reactions, which maintain the orientations of the structure upon intercalation. This aspect signifies that the intercalation into layered materials is prone to be highly reversible, making the interlayers versatile hosts for the insertion of various ions and molecules. This is a characteristic feature that distinguishes layered materials from other types of hosts with 1D or 3D channels for guest

Energy and Environment Series No. 23
Magnesium Batteries: Research and Applications
Edited by Maximilian Fichtner

Published by the Royal Society of Chemistry, www.rsc.org

ions. As a result, layered materials have been key players in many successful devices for electrochemical energy storage, such as graphite and lithium transition metal oxides in lithium-ion batteries, just to name a few.

Considering these aspects, it was a natural consequence to consider layered materials as promising cathodes for rechargeable magnesium batteries. Since magnesium rechargeable batteries utilize a magnesium metal anode, it was preferable to consider bare transition metal chalcogenides without Mg in their pristine structure. Such transition metal chalcogenides include layered materials such as titanium disulfide (TiS_2), molybdenum disulfide (MoS_2), and vanadium pentoxide (V_2O_5), which have been efficient intercalation hosts for Li^+. However, non-layered, Chevrel-phase molybdenum chalcogenides ($Mo_6S_{8-x}Se_x$) were the only known cathodes that intercalate Mg^{2+} efficiently,[4,5] until the recent discoveries of other selenides and sulfides that intercalate Mg^{2+} at 25 and 60 °C, respectively.[6–8]

Despite the highest redox potentials and theoretical capacities of oxides among the chalcogenides, the highly electrophilic nature of the oxides results in severe side reactions with magnesium ion electrolytes that are often nucleophilic. Moreover, the smallest ionic diameter and number of core electrons in oxygen among the group VI elements brings about strong electrostatic interactions of divalent Mg^{2+} ions with oxide ions in the solid-state, as well as with counterions in electrolytes. As a result, the intercalation of divalent Mg^{2+} is greatly hindered in layered oxides, despite the diagonal relationship between Li^+ and Mg^{2+} that predicts similar chemical properties (Figure 7.1a). In more detail, Mg^{2+} must be desolvated or dissociated from counterions to

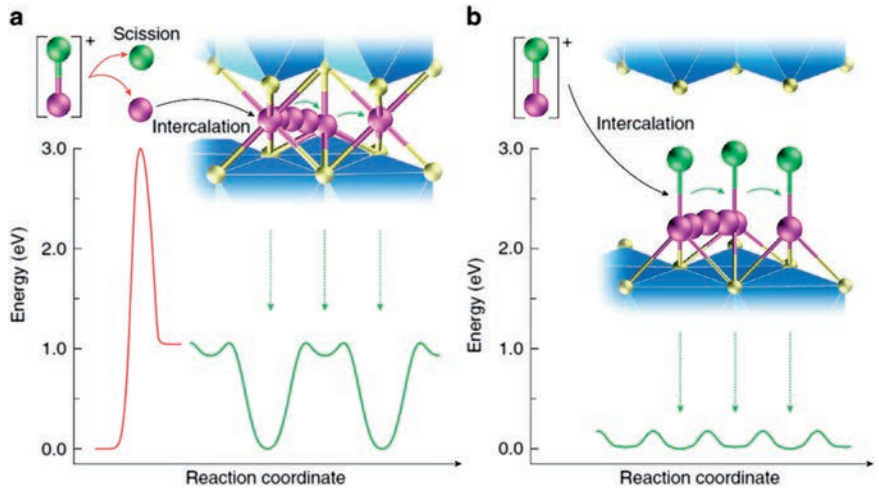

Figure 7.1 Energy diagrams for the intercalation and diffusion of (a) Mg^{2+} and (b) $MgCl^+$ in a sulfide host. Purple, green, and yellow balls represent Mg, Cl, and S atoms, respectively. Reproduced from ref. 9, https://doi.org/10.1038/s41467-017-00431-9, under the terms of the CC BY 4.0 licence, http://creativecommons.org/licenses/by/4.0/.

initiate the intercalation, which often requires more than 3 eV per Mg atom. Moreover, the desolvated Mg^{2+} must overcome a large diffusion barrier of *ca.* 1 eV per Mg atom, which is far beyond what can be readily achieved at room temperature.[9]

Due to the sluggish kinetics of the intercalation and diffusion of divalent Mg^{2+} into layered oxides, other more facile side reactions often prevail. This aspect provides a significant possibility for the co-intercalation of undesirable species, which interferes with the genuine intercalation of Mg^{2+}. Recent rigorous compositional and structural characterization found that a substantial portion of the electrochemical activity in hydrated Mg^{2+} electrolytes is actually due to the intercalation of protons,[10–12] although previous literature studies have assumed that the electrochemical activity was evidence for the intercalation of Mg^{2+}. In this respect, it will be meaningful to look back on the history of research on layered hosts for the intercalation of Mg^{2+}. In addition to the retrospective information on layered cathodes for Mg^{2+}, this chapter also summarizes and discusses conversion-type cathodes for Mg^{2+} as a newer avenue.

7.2 Materials for Intercalation

Because a separate chapter will be dedicated to cathodes with spinel structures, this part will mainly focus on layered intercalation hosts.

7.2.1 Layered Sulfides and Selenides

Sulfides and selenides are compatible in Mg^{2+} electrolytes wherein a Mg metal anode can be operated, because they are less electrophilic compared with oxides. This aspect enables full cell operation using cathodes based on sulfides or selenides, despite their relatively lower theoretical voltage and capacity than oxides. Moreover, the larger ionic diameter leads to weaker electrostatic interactions with Mg^{2+}, enabling more facile kinetics to intercalate Mg^{2+}. As a result, these materials are relatively free from the debates on genuine Mg^{2+} intercalation. There is solid proof for genuine intercalation of Mg^{2+} in sulfides and selenides, such as in Chevrel-phase Mo_6S_8, TiS_2, and MoS_2. On the other hand, the operational voltage is limited to *ca.* 1 V *vs.* Mg/Mg^{2+}, making them impractical for commercialization. Therefore, the main usage of sulfides and selenides has been the testing of general strategies and ideas to enhance the electrochemical performances to store Mg^{2+}.

Layered TiS_2 is a representative intercalation host that was reported by Whittingham in 1976.[13] However, intercalation of Mg^{2+} into layered TiS_2 has been substantially difficult because of the large migration energy barrier.[9] As a result, the reversible capacity is limited to *ca.* 20 mA h g^{-1} at room temperature. On the other hand, more facile intercalation has been proven at 60 °C, giving rise to *ca.* 160 mA h g^{-1} by overcoming the migration barrier at a higher operational temperature. Expansion of the interlayer by larger organic cations, namely 1-butyl-1-methylpyrrolidinium ($PY14^+$) has enabled

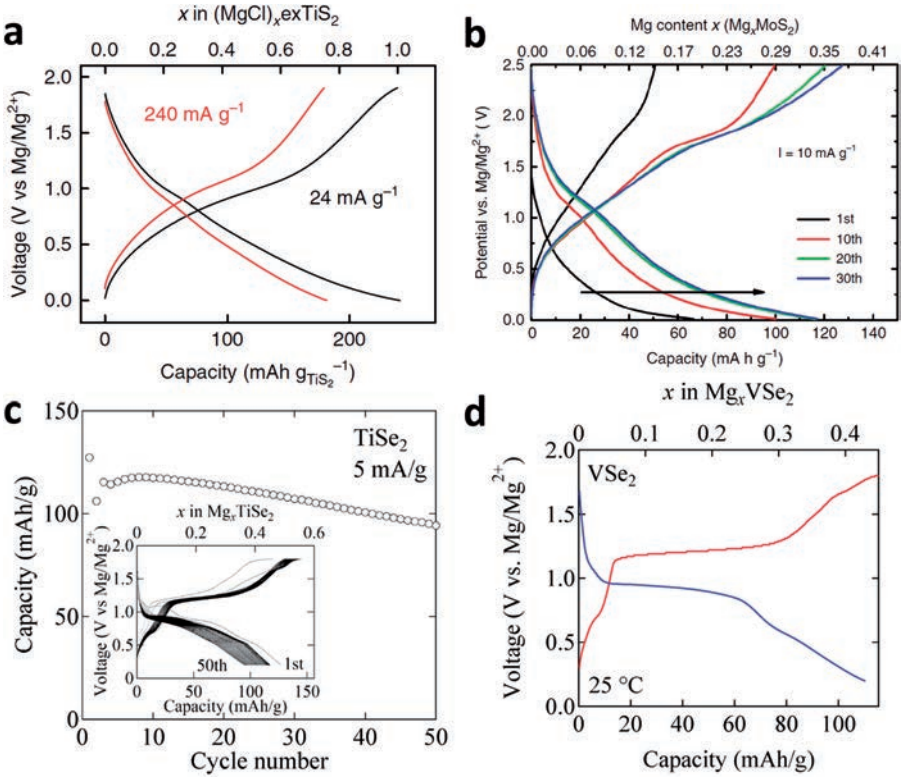

Figure 7.2 Voltage profiles of layered sulfides and selenides in a full cell coupled with a Mg metal anode at room temperature. (a) Expanded TiS_2, (b) MoS_2/C composite, (c) $TiSe_2$ and (d) VSe_2. Reproduced from ref. 6, https://doi.org/10.1038/s41467-018-07484-4, ref. 9, https://doi.org/10.1038/s41467-017-00431-9, and ref. 16, https://doi.org/10.1038/srep12486, under the terms of the CC BY 4.0 licence, http://creativecommons.org/licenses/by/4.0/.

an enhanced capacity that is close to the theoretical value of *ca.* 240 mA h g^{-1} and excellent rate capability at room temperature by the intercalation of $MgCl^+$ (Figures 7.1b and 7.2a).[9]

MoS_2 is another representative layered sulfide that is known to intercalate lithium ions reversibly. However, Mg^{2+} intercalation is sluggish due to the strong electrostatic forces that exist between the divalent Mg^{2+} ions and sulphur anions. The interlayer expansion through pillaring with polymer was shown to be effective to facilitate the diffusion of Mg^{2+} in the host materials,[14] although the strategy of expanding the interlayer has drawbacks in the form of a lower cell voltage.[15] The utilization of solvated Mg^{2+} into nanosized 1T-phase MoS_2 also enabled a much larger capacity at room temperature, by coupling of three factors: screening of divalent ions, high electronic conductivity, and decrease in the diffusion length (Figure 7.2b).[16] It is possible that further engineering of the size of organic cations or solvent molecules may enhance the electrochemical performance. On the other hand, the selenides

$TiSe_2$ and VSe_2 deliver capacity of *ca*. 110 mA h g^{-1} at room temperature without any special treatment, in accordance with general tendencies of chalcogenides (Figure 7.2c and d).[6] Also, doping selenium into other chalcogenides may further facilitate the kinetics of Mg^{2+} intercalation, as shown in the previous example with Chevrel phase $Mo_6S_{8-x}Se_x$.[5]

7.2.2 Layered Oxides

7.2.2.1 Vanadium Oxide (V_2O_5)

Since the pioneering electrochemical and chemical screening of various cathodes by T.D. Gregory *et al.*,[17] a group of European researchers took initiative to find potential cathodes for Mg batteries. P.G. Bruce *et al.* conducted more rigorous chemical magnesiation using di-*n*-butylmagnesium ($(C_4H_9)_2Mg$) as a reducing agent, with which he found several candidates, including V_2O_5, which can possibly intercalate Mg^{2+}.[18] P. Novák *et al.* focused on electrochemical studies on oxides based on vanadium and molybdenum, using organic electrolytes based on magnesium perchlorate ($Mg(ClO_4)_2$) salt and propylene carbonate (PC) or acetonitrile (AN) solvents.[19–21] They concluded that a crystal of V_2O_5 hardly intercalates Mg^{2+}, but porous electrodes based on powder deliver a high capacity of *ca.* 180 mA h g^{-1} if water is added in the electrolyte to a concentration of *ca.* 1 M. However, it was unclear whether the capacity originates from the intercalation of Mg^{2+} or not. During the initial stage of research, only a few researchers were aware of the possible side reactions other than the intercalation of Mg^{2+} in non-aqueous electrolytes containing water. The electrochemical tests with $Mg(ClO_4)_2$ salt had severe pitfalls as the salt is highly hygroscopic, so the electrolytes are prone to contain water moieties. In this respect, less hygroscopic magnesium trifluoromethylsulfonylimide ($MgTFSI_2$) salt was more useful in the electrochemical tests.

Amatucci *et al.* claimed that nanosized V_2O_5 is capable of intercalating Mg^{2+} based on electrochemical tests only.[22] Similarly, Gershinsky *et al.* utilized a thin film electrode with facilitated electrode kinetics.[23] However, there was a pitfall in that the thin film was much more susceptible to trace amounts of water because the total amount of water in the electrolyte was sufficient enough to interfere with such small amount of electrode material. Based on the initial results, a couple of companies targeted the development of full battery cells with a V_2O_5 cathode and Mg anode. Pellion technologies invented a method that is claimed to facilitate the solid-state diffusion of Mg^{2+} by expanding the interlayer distance with the intercalation of larger organic cations in the interlayer.[24] They claimed that partial expansion of the interlayer distance resulted in an enhancement of the reversible capacity based on the electrochemical and spectroscopic characterizations; however, more rigorous studies are needed regarding the potentially profitable roles of organic cations in V_2O_5 for the intercalation of Mg^{2+}. T. S. Arthur *et al.* at the Toyota Research Institute North America claimed enhanced electrochemical storage of Mg^{2+} by amorphization and manipulation of the interlayer distance of V_2O_5 by compositing with phosphorus pentoxide (P_2O_5).[25]

There have been continuous reports that water in the electrolyte or in the crystal structure plays significant roles in enhancing the capacity of V_2O_5 in Mg^{2+} electrolytes.[26–28] In particular, a V_2O_5 aerogel containing structural water has shown a large capacity of up to 542 mA h g^{-1} in AN-based Mg^{2+} electrolytes.[29–32] In some cases, the Mg content was shown to increase in accordance with the electrochemical reduction, although some perchlorate ions were detected along with Mg^{2+}, leaving the possibility for co-intercalation of $MgClO_4^+$ ions.[30]

Since 2013, the Joint Center for Energy Storage Research (JCESR) team initiated rigorous and critical studies on α-V_2O_5. However, the electrochemical and spectroscopic tests revealed that the actual Mg content was small and the intercalation of protons prevailed, especially as observed from solid-state nuclear magnetic resonance (NMR) spectroscopic measurements.[10] Two research groups conducted rigorous structural analysis of the electrochemically reduced product in hydrated Mg^{2+} electrolytes with XRD, finding that the intercalated species was dominated by protons rather than Mg^{2+} ions.[11,12] These findings even led to the serious question of whether α-V_2O_5 is able to intercalate Mg^{2+} or not. Recently, S.-T. Hong *et al.* claimed that Mg content was linearly proportional to the state of charge (SoC) for layered $V_3O_7{\cdot}H_2O$ that contains structural water (Figure 7.3).[28] However, it has not been possible to cycle such hydrated materials with structural water in Mg^{2+} electrolytes that can operate a Mg metal anode, probably due to the chemical reactivity of such Mg^{2+} electrolytes towards oxides or due to the leakage of structural water into the electrolyte that may lead to severe degradation of the Mg metal anode.

In summary, layered V_2O_5 has been regarded as a potentially ideal candidate for a Mg cathode; however, it is under a serious test to determine if it can be a Mg battery cathode or not. The added water may have been the source of protons, against the previous explanation of enhanced capacity in

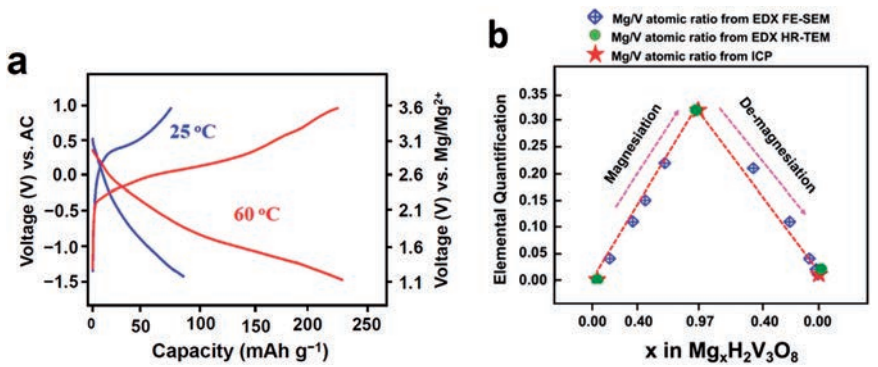

Figure 7.3 Voltage profiles of the layered $V_3O_7{\cdot}H_2O$ at 25 and 60 °C, and (b) the linearly proportional Mg content to the state of charge. Reproduced from ref. 28 with permission from American Chemical Society, Copyright 2018.

wet electrolytes by electrostatic screening of divalent Mg^{2+} ions with water dipoles.[26] These debates await direct proof or disproof of its inherent ability to intercalate Mg^{2+} in the absence of water moieties.

7.2.2.2 Molybdenum Oxide (MoO_3)

Generally, the strategies to enhance V_2O_5 have also been applied to layered MoO_3, such as a thin film approach and interlayer expansion.[23,24] Theoretical and experimental studies have shown that doping with fluorine could enhance the reversible capacity.[33,34] However, protons may have played a significant role in the reversible capacity as in the case of V_2O_5.

7.2.3 Graphite

To overcome the limitations in the available electrolytes that are compatible with magnesium metals, insertion electrodes of Mg^{2+} ions with a low redox potential have emerged as alternative negative electrode materials. These insertion electrodes are capable of being applied in conventional electrolytes such as $Mg(TFSI)_2$, $Mg(PF_6)_2$ or $Mg(CF_3SO_3)_2$, free from corrosive chloride ions (Cl^-).[35–37] Moreover, the use of intercalation electrodes is beneficial in terms of structural and chemical integrity compared to alloying compounds such as Sn, and Bi, which suffer from drastic pulverization caused by large volumetric changes upon repeated alloying and de–alloying processes. Pontiroli *et al.*[38] first discovered that Mg^{2+} ions can reversibly intercalate into fullerene (C_{60}), forming Mg_2C_{60}, which has the same bonding architecture as the lithiated fulleride Li_4C_{60}.[38,39] This report initiated other research studies on the possibility of the formation of a Mg^{2+}–intercalated graphite intercalation compound (GIC) in a similar manner to how Li^+ forms LiC_6 with graphite.[40,41] K. T. Lee *et al.*[40] have found that Mg^{2+} ions are reversibly intercalated into graphite together with linear ether solvents such as diethylene glycol dimethyl ether (DEGDME) and 1,2-dimethoxyethane (DME). A similar phenomenon has also been reported in the incorporation of Li^+ and Na^+ ions into graphite layers.[42–46] For example, solvated Li^+ ions in propylene carbonate (PC) are known to intercalate into graphite to form a ternary compound, $Li_x(PC)_yC_n$.[47] Density functional theory (DFT) calculations shows that Mg^{2+} ions strongly bind to linear ethers, particularly DEGDME and DME (binding energies are estimated to be 10.05 and 7.60 eV, respectively), enabling co-intercalation of these ion–solvent pairs into the graphene layers. On the other hand, the binding energies for Mg^{2+}–ethylene carbonate (EC) and Mg^{2+}–diethyl carbonate (DEC) complexes are substantially lower, alluding that de-solvation of Mg^{2+} ions should occur at the electrolyte/graphite interface in this case. The DFT calculations also revealed that the intercalation of Mg^{2+}–DEGDME into graphite is a thermodynamically favorable process and furthermore, the formation of a double-layer structure between graphene layers is favored over that of a single-layer (Figure 7.4), similar to the case

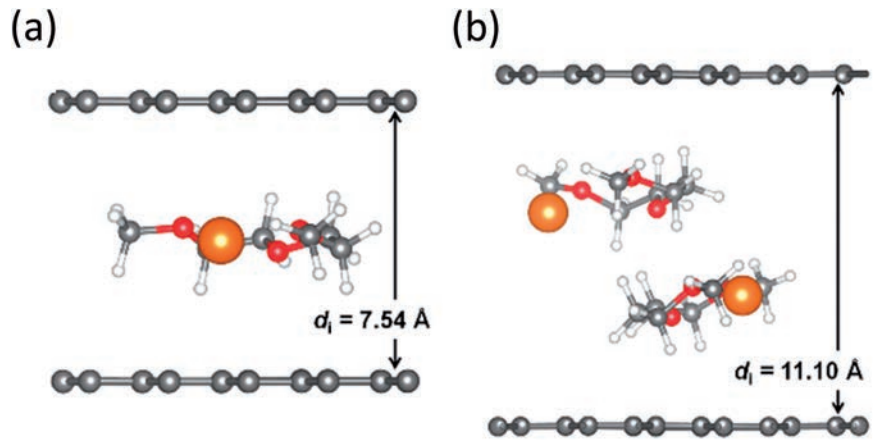

Figure 7.4 Schematic of the Mg^{2+}–DEGDME co-intercalated graphite: (a) single- and (b) double-layer structures. Orange, white, gray, and red balls represent Mg, H, C, and O atoms, respectively. d_i represents the intercalant gallery height. Reproduced from ref. 40 with permission from American Chemical Society, Copyright 2018.

of Na^+–DEGDME co-intercalation into graphite.[48] It is noteworthy that the diffusivity of the Mg^{2+}–DEGDME complex into graphite layers is estimated to be 1.5×10^{-8} cm^2 s^{-1} at room temperature, comparable to that of Li^+ in graphite (1.8×10^{-9} cm^2 s^{-1}).[40] This indicates that the kinetics involved in the co-intercalation of the Mg^{2+}–DEGDME complex are as fast as Li^+ ion intercalation into graphite, suggesting that graphite may be utilized as a high-rate anode material. The galvanostatic cycling of a Mg/graphite cell with 0.3 M of $Mg(TFSI)_2$ in DME/DEGDME solvent exhibited reversible voltage profiles with a constant capacity of ~180 mA h g^{-1}. A rather high polarization (>2 V) even at a low current rate during cycling is speculated to originate from the slow kinetics for Mg stripping/plating on the Mg electrode in this electrolyte, not from the intercalation of Mg^{2+}–DEGDME complexes into graphite layers. A galvanostatic intermittent titration technique (GITT) measurement indicated that the approximate redox potential for co-intercalation of Mg^{2+}–DEGDME into graphite is surprisingly 1 V *vs.* Mg/Mg^{2+}.[40] Therefore, a drastic improvement in the performance actually enables graphite to be considered as a positive electrode material. The mechanistic study analyzed by *ex situ* X-ray diffraction patterns of the electrodes at various charge–discharge states reveals that co-intercalation of Mg^{2+}–DEGDME exhibits a well-known staging behavior of graphite,[46,49,50] signifying that Mg^{2+} ions intercalate every *n*th space between the graphene layers. The theoretical intercalant gallery height from the double-layer structure (11.10 Å) is in good agreement with the value experimentally estimated (11.45 Å) of the fully discharged graphite at stage number 5.[46] Fourier-transform infrared (FT–IR) studies also indicated the presence of DEGDME molecules in the fully discharged electrode. Transmission electron microscope studies showed that a Mg-rich disordered region is observed after the intercalation of Mg^{2+} ions. These amorphous phases

account for a rather high discharge capacity (180 mA h g^{-1}) compared with the calculated value from the graphite intercalation compound at stage number 5. Schmuck *et al.*[41] investigated Mg^{2+} intercalation into natural graphite in 0.5 M $Mg(TFSI)_2$/*N*,*N*-dimethylformamide (DMF) electrolyte, delivering a low but steady reversible discharge capacity of ~30 mA h g^{-1}. From *ex situ* XRD pattern analysis, they observed that Mg^{2+} intercalation produces a staging compound, but it was not clearly identified whether co-intercalation of DMF solvent occurs. It is noteworthy that in many cases, co-intercalation of solvent molecules with metal cations is prone to triggering irreversible exfoliation of graphite that will gradually deteriorate the electrochemical performance.[51,52] This aspect of the co-intercalation of Mg^{2+}–solvent pairs should be further investigated.

7.2.4 $VOPO_4$

A report by Yao *et al.*[53] proposed that the expansion of the interlayer spacing of layered TiS_2 by pre-intercalation of large $PY14^+$ cations enables the intercalation of a $MgCl^+$ species rather than Mg^{2+} ions. This lowers the activation barrier for ion migration and saves the dissociation energy (E_a) related to the dissociation of $MgCl^+$ into its component species, which could amount for at least 3 eV. This report opened up a new opportunity in that other layered compounds (metal chalcogenides or metal oxides) could also be potentially utilized as positive electrode materials by applying a similar strategic approach. $VOPO_4$ has a two-dimensional layered structure consisting of a polyanion framework, where VO_6 octahedra are linked to PO_4 tetrahedra by sharing corners to form two-dimensional layered structures (Figure 7.5).[54–56] This material has been proven to be an excellent cathode material for Li- or Na-ion batteries.[57–59] The hydrated phase with interlayer water molecules, $VOPO_4{\cdot}nH_2O$ (termed as OH–$VOPO_4$, n is typically 2) can be readily prepared *via* a hydrothermal method.[60] The typical interlayer distance in OH–$VOPO_4$ is 7.41 Å.[56,58] These $VOPO_4{\cdot}2H_2O$ particles were subjected to ultrasonic agitation to be exfoliated in water, followed by incorporation of phenylamines, allowing a self-assembly process to occur in phenylamine, producing $VOPO_4$

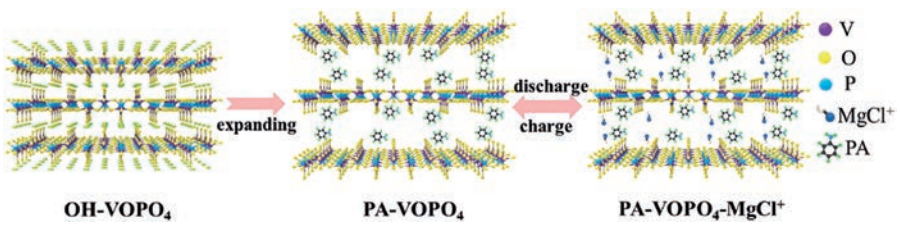

Figure 7.5 Schematic illustration of the layer expanded $VOPO_4$ by phenylamine, and proposed reaction mechanism of PA–$VOPO_4$ nanosheets as Mg^{2+} ion-storage materials. Reproduced from ref. 60 with permission from John Wiley and Sons, © 2018 WILEY-VCH Verlag GmbH & Co. KGaA, Weinheim.

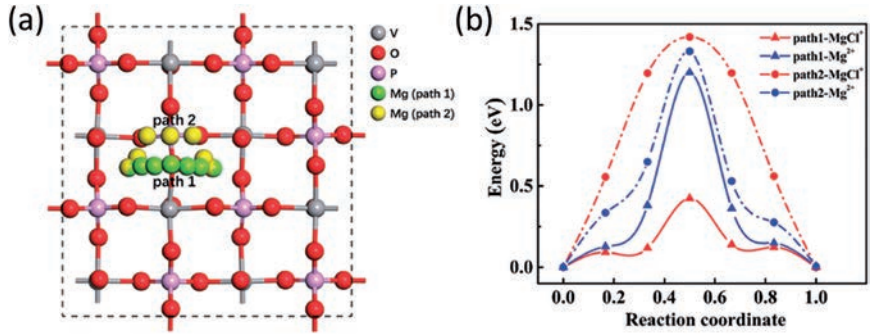

Figure 7.6 (a) Possible diffusion paths and (b) corresponding activation energy barrier profiles for Mg^{2+} or $MgCl^{+}$ migration in PA–$VOPO_4$ nanosheets. Reproduced from ref. 60 with permission from John Wiley and Sons, © 2018 WILEY-VCH Verlag GmbH & Co. KGaA, Weinheim.

nanosheets with a vastly expanded interlayer spacing of 14.2 Å (termed as PA–$VOPO_4$). The expansion of layers was confirmed by a significant shift in the (001) reflection in the XRD diffraction pattern to a lower angle and measurement of the interlayer distance directly from high-resolution TEM images. The existence of phenylamine in the interlayer was clearly evidenced by comparative analyses of EDS, FT–IR and TGA results for OH– and PA–$VOPO_4$. This structural reconfiguration of $VOPO_4$ led to remarkable enhancement in the electrochemical performance, especially in the rate performance, where the reversible discharge capacity was observed to be 310 mA h g^{-1} at 50 mA g^{-1} even after 500 cycles. The discharge capacity at 2000 mA g^{-1} was still found to be 100 mA h g^{-1}. The change in the electrode mass containing PA–$VOPO_4$ after various stages of discharge reactions indicates that it is $MgCl^{+}$ that intercalates into layers for PA–$VOPO_4$, while un-solvated Mg^{2+} ions are inserted into the layers of OH–$VOPO_4$. Furthermore, X-ray photoelectron spectroscopic (XPS) spectra and energy dispersive X-ray spectroscopic (EDS) analysis for the discharged electrode concurrently showed the existence of both Mg and Cl species in a roughly 1 : 1 ratio in the discharged electrode. First-principles calculations based on DFT showed a substantial difference in the activation energy, E_a, for ion migration in PA–$VOPO_4$, *i.e.* 0.42 eV for $MgCl^{+}$ diffusion and 1.20 eV for Mg^{2+} along the P1 pathway shown in Figure 7.6,[60] indicating that much higher diffusion kinetics are expected for $MgCl^{+}$ than for Mg^{2+}. This study hints that other layered compounds could be expanded to improve their performance by taking a similar approach.

7.2.5 VS_4

Z. Jin *et al.*[61] reported that vanadium tetrasulfide (VS_4) is a favorable cathode material that acts as a facile intercalation host for Mg^{2+} ions. VS_4 has a peculiar one-dimensional chain-like crystal structure similar to the

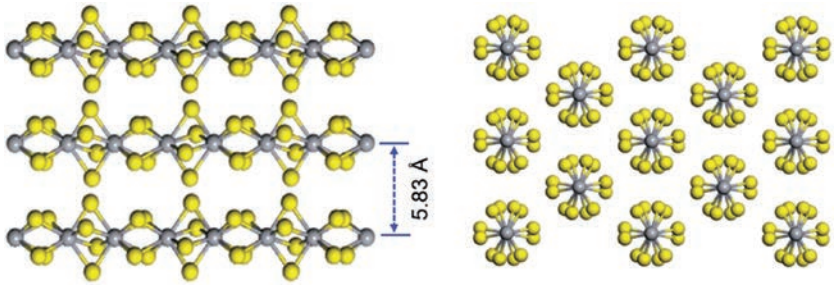

Figure 7.7 Schematic crystal structure of VS_4. (mineral patronite). Lateral-view (left) and vertical-view (right) of the one-dimensional chain-like crystalline structure of VS_4, exhibiting an interval of 5.83 Å between the atomic chains. Reproduced from ref. 61 with permission from John Wiley and Sons, © 2018 WILEY-VCH Verlag GmbH & Co. KGaA, Weinheim.

mineral patronite, where V^{4+} is coordinated to four disulfide anions (S_2^{2-}) along the c-axis (Figure 7.7).[62–64] These atomic chains are 5.83 Å apart from each other, which is much larger than the ionic diameter of Mg^{2+} ion (~1.44 Å), and are only weakly bound by van der Waals forces. They have shown that Mg^{2+} ions can readily pass through the open channels formed by these atomic chains.[61] Electrochemical insertion of Li^+ and Na^+ ions into these 1D channels in VS_4 was investigated previously.[65–68] Nanodendrites of VS_4 prepared by a solvothermal method exhibited an initial discharge capacity of 251 mA h g^{-1} at a current rate of 100 mA g^{-1} and stable cycling performance up to 800 cycles with a current density of 500 mA g^{-1}. XPS studies on the electrode at various stages of discharge and charge states indicated that the insertion of Mg^{2+} ions into VS_4 led to the partial oxidation of V^{4+} to V^{5+}, and a partial reduction of S_2^{2-} to S^{2-}, while the extraction of Mg^{2+} ions from the channels caused V^{5+} and S^{2-} to revert back to V^{4+} and S_2^{2-}. Insertion of Mg^{2+} ions into channels in VS_4 was verified analytically by *ex situ* TEM, XRD and Raman spectroscopy for the electrode at various stages of discharge and charge states. From the XRD and HR–TEM studies on both the discharged and charged electrodes, little variation in the lattice parameters was observed after the insertion of Mg^{2+} ions into VS_4, in an accordance with the results from DFT calculations. The fact that no significant morphological changes were observed during the insertion process, and that MgS and elemental vanadium were not observed after full discharge strongly indicates that the intercalation of Mg^{2+} ions is mainly responsible for the reaction mechanism. This is distinctly different from the behavior observed for a Li–VS_4 battery,[64] where Li_2S and elemental V were observed after full reduction by means of a conversion process. In a Mg–VS_4 battery, the original topotactic structure is well maintained, which is beneficial to the reversibility and cycling life of this battery system.

7.2.6 Prussian Blue Analogues

Prussian Blue Analogues (PBAs) feature a wide open framework with the general formula, $A_xMM'(CN)_6{\cdot}yH_2O$ (A = metal ions, M = Fe, Ni, Mn, V, Mo, Cu, Co; M′ = Fe, Co, Cr, Ru).[69,70] The crystal structure of PBAs are analogous to those of ReO_3 or ABX_3 perovskites, where the A sites are filled with A cations as well as zeolitic water molecules, and the B sites are systematically occupied by M^{m+} and M'^{n+} ions bridged by cyano (C≡N) ligands along the edges (Figure 7.8). It is known that small molecules or ions, 0 to 2 per formula unit, can be incorporated into the A sites of the large open cages, leading to corresponding changes in the oxidation states of the M and M′ ions.[71–74] Y. Cui *et al.*[75–77] reported various types of PBAs as possible cathode materials for monovalent (Li^+, Na^+, K^+) or multivalent (Mg^{2+}, Ca^{2+}, Sr^{2+}, Ba^{2+}) cathode materials with a high rate capability and a long cycling life. In particular, they showed that nickel hexacyanoferrate ($KNiFe^{3+}(CN)_6$, NiHCF) can function as an efficient cathode material with a long cycling life and high energy efficiency in aqueous electrolyte.[75] In NiHCF, half of the A sites are occupied by K^+ ions, and Ni^{2+} and Fe^{3+} fill the N-coordinated M sites, and C-coordinated M′ sites, respectively. The discharge–charge curves for NiHCF with an aqueous electrolyte show a sloping potential, indicating that a single phase reaction occurs. They postulated that the partial shielding of electrostatic interactions by the water molecules located at the A sites and ferricyanide vacancies with a diameter of 5 Å are responsible for the facile intercalation kinetics of divalent cations into NiHCF. Hong *et al.* carried out a related study using NiHCF with a composition of $K_{0.86}Ni[Fe(CN)_6]_{0.954}(H_2O)_{0.766}$, but in an organic electrolyte, 0.5 M $Mg(ClO_4)_2$ in acetonitrile with a thick carbon black anode.[70] Xia employed a NiHCF cathode and polyimide anode to construct a

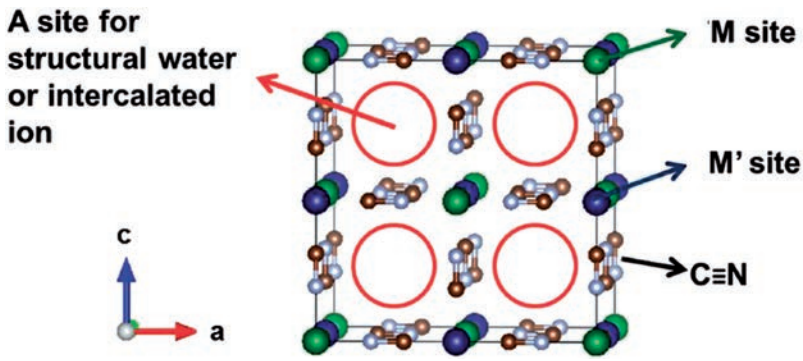

Figure 7.8 Schematic crystal structure of a Prussian Blue analogue, A_xM-$M'(CN)_6{\cdot}yH_2O$. The structure is analogous to that of an ABX_3 perovskite or ReO_3. Reproduced from ref. 71, https://doi.org/10.1002/advs.201600044, under the terms of the CC BY 4.0 licence, https://creativecommons.org/licenses/by/4.0/.

supercapacitor-like high-power cell with a 1 M $MgSO_4$ aqueous electrolyte.[78] They obtained a remarkable cycling performance of up to 5000 cycles with an excellent rate performance.

7.3 Materials Based on Conversion and Displacement Reactions

7.3.1 Advantages of Conversion/Displacement Reactions for Mg^{2+} Storage

The adoption of intercalation compounds (graphite and layered transition metal oxides) as electrode materials plays a crucial role in securing the high performance and safety of battery cells required for the commercialization of Li-ion batteries. However, that is not the case with the intercalation of divalent Mg^{2+} ions into host materials. One of the main roadblocks is that it induces a strong coulombic interaction with the framework of the host materials, leading to a high activation barrier for ion migration and consequently, poor reaction kinetics.[79,80] Expanded layered compounds with a large interlayer spacing, such as $PY14^+$-intercalated TiS_2, showed one possible direction to pursue in order to overcome this issue through facilitating the incorporation of $MgCl^+$ instead of Mg^{2+} ions, markedly lowering the electrostatic interactions between the host and guest.[53] However, from a practical point of view, this approach requires concentrated electrolytes, that are abundant in chloride ions, otherwise chloride ions may be depleted from the electrolyte causing changes in the insertion mode or a sudden drop in the ionic conductivity of the electrolyte as the discharge process proceeds. Furthermore, a wide expansion of the interlayer spacing may result in low volumetric capacity, even lower than the conventional Mo_6S_8 Chevrel phase (519 Ah L^{-1}). Conversion-type reactions could provide an alternative reaction pathway to circumvent this situation.[81–83] In this case, a new phase, which bears little or no topotactic relationship to the original material, arises as a result of the reaction with Mg^{2+} ions. Conversion reactions usually proceed slowly as the reaction occurs only at the phase boundaries among the involved phases. However, the reaction kinetics of a conversion-type reaction can be significantly enhanced by reducing the particle size to the nanoscale as they provide much larger reaction sites and a shorter diffusion length for the full utilization of the original particles.[84,85] For some transition metal chalcogenides bearing a close structural kinship with MgS or MgSe with a rock-salt structure, a displacement reaction has been proposed to account for the high reversible capacity and fast diffusion kinetics at room temperature. In this reaction, insertion of Mg^{2+} ions result in the replacement of transition metal ions in the cathode material by Mg^{2+} ions, and the extrusion of transition metal in the form of nanocrystals. The high mobility of some transition metal ions and weak interaction of hard acid Mg^{2+} ions with soft base

anions such as S^{2-} or Se^{2-} (based on hard–soft acid–base (HSAB) theory) can promote the displacement reaction.[85–87] Since the overall anion structure is preserved during the process, a displacement reaction typically involves less irreversible capacity and a smaller overpotential compared to conventional conversion reactions. In both cases, the preparation of nanosized or nanostructured materials is the most important factor to successfully accomplish fast reaction kinetics. Recently, copper chalcogenides with a variety of crystal structures have been extensively studied for the possibility of using these compounds as conversion-type cathode materials for rechargeable Mg batteries.

7.3.2 Copper Chalcogenides

A series of copper chalcogenides, $Cu_\alpha X$ ($1< \alpha < 2$, X = S, Se), such as CuS, Cu_2S, and Cu_2Se have been proposed as promising cathode materials for rechargeable Mg batteries.[88–91] When applied as cathode materials in rechargeable Mg batteries, these are known to undergo conversion or displacement reactions, producing Cu metal and MgS or MgSe as discharge products. These materials have gained attention since they show a relatively small overpotential at room temperature, comparable to that of other efficient cathode materials based on intercalation chemistry. The practical voltage from these conversion reactions typically ranges from 1.0 to 1.5 V.

CuS has a hexagonal crystal structure analogous to the mineral covellite, and its theoretical capacity from full conversion into elemental Cu and MgS amounts to 560 mA h g^{-1}.[92] Nazar *et al.*[88] was the first to report that CuS can store Mg ions up to 200 mA h g^{-1} in an all-phenyl-complex electrolyte at 150 °C. Mai *et al.*[89] demonstrated that CuS nanospheres can deliver a high discharge capacity of over 360 mA h g^{-1} at room temperature by applying $Mg(ClO_4)_2$ in acetonitrile as an electrolyte system, although they had to use a thick carbon black anode due to the incompatibility of their electrolyte with Mg metals. XRD and XPS studies on the electrodes at various stages verified that this electrode works based on a conversion reaction mechanism. Two-step reactions as suggested below have been proposed as Cu_2S appears as an intermediate species during the electrochemical process. Cu_2S is speculated to undergo a conversion reaction with Mg^{2+} ions.[89]

$$2CuS + Mg^{2+} + 2e^- \leftrightarrow Cu_2S + MgS$$

$$Cu_2S + Mg^{2+} + 2e^- \leftrightarrow 2Cu + MgS$$

$Cu_{2-\delta}S$ has a wide variety of crystal structures with significant nonstoichiometry in its composition. The theoretical capacity from its full conversion into Cu and MgS amounts to 337 mA h g^{-1}.[93] Miyasaka *et al.*[90]

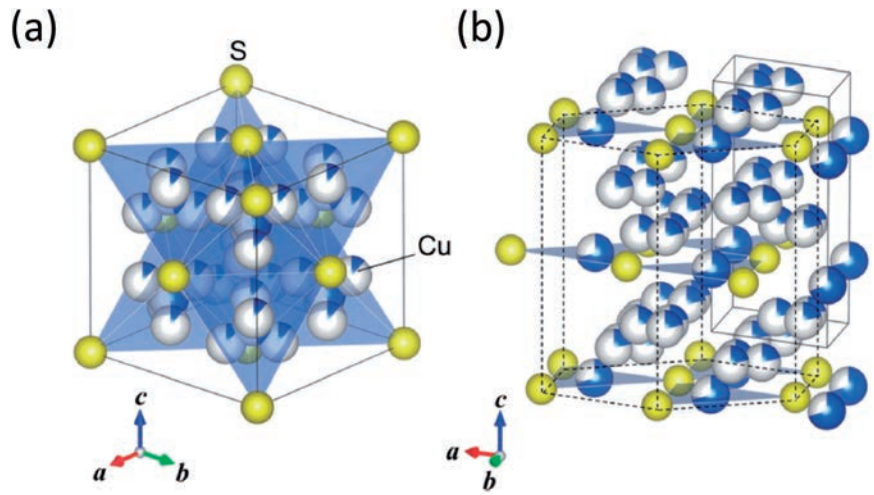

Figure 7.9 A comparison of the crystal structure of cubic and hexagonal $Cu_{2-\delta}S$. (a) In cubic digenite (h-$Cu_{2-\delta}S$), anions are arranged in a face-centered cubic lattice, where Cu ions are distributed at tetrahedral or trigonal sites. The blue polyhedra represent tetrahedral sites. (b) In hexagonal chalcocite (h-$Cu_{2-\delta}S$), the anions make up a hexagonal close-packed lattice, where Cu ions are distributed at the interstitial sites. Reproduced from ref. 90 with permission from The Chemical Society of Japan, Copyright 2017.

evaluated the effect of these crystal structures of $Cu_{2-\delta}S$ on its performance as a cathode material for a rechargeable Mg battery. They proposed that the cubic phase (mineral digenite), which have an analogous anion lattice to that of MgS (Figure 7.9), undergoes a facile displacement reaction to account for its low overpotential, even at room temperature. On the other hand, a conversion mechanism also works for the hexagonal phase (mineral chalcocite), whose structure is unrelated to that of MgS. A nanocomposite formation with conductive carbon improved the reversible capacity up to ~200 mA h g^{-1}.

Miyasaka *et al.*[91] investigated β-Cu_2Se as a displacement–type cathode material for Mg batteries. In β-Cu_2Se, Se atoms are arranged in a face centered cubic structure, which is the same arrangement as for MgSe (Figure 7.10). Cu atoms are located randomly at tetrahedral and trigonal sites. In this structure, Cu^+ ions are known to be highly mobile, so that β-Cu_2Se is considered as a superionic conductor. The displacement reaction between Li^+ and Na^+ ions was reported previously.[94,95] Nanocrystallites (~100 nm) of β-Cu_2Se were prepared *via* a solution-based method, delivering a reversible discharge capacity of around 230 mA h g^{-1}. From the XRD observations, MgSe and Cu were mainly found in the fully discharged electrode, although several other phases such as α-Cu_2Se, and Cu_3Se_2, which is structurally related to β-Cu_2Se, were also found.

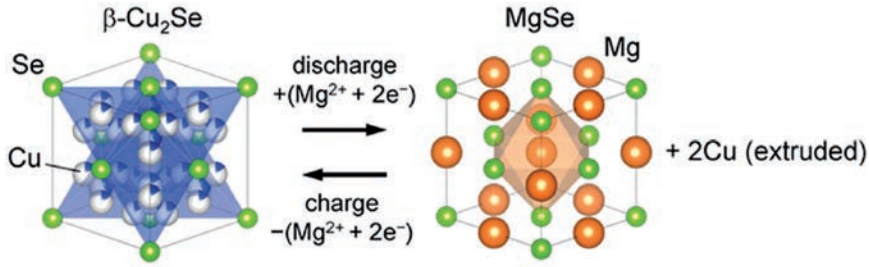

Figure 7.10 Crystal structure of β-Cu_2Se and a schematic for the displacement reaction with Mg^{2+} ions. In β-Cu_2Se, the Se anions take a face-centered cubic arrangement, where Cu ions are distributed randomly at the trigonal or tetrahedral sites. MgSe has the same anion arrangement as β-Cu_2Se. During the displacement reaction, Mg^{2+} ions are incorporated into the octahedral sites, while Cu ions are extruded from the interstitial sites to form Cu metal. Reproduced from ref. 91 with permission from Elsevier, Copyright 2016.

7.4 Conclusion

Insertion cathodes for magnesium batteries are under continuous investigation by researchers worldwide who are aiming at understanding and developing multivalent battery chemistry as a more sustainable technology for energy storage and electromobility. Recent clarification of the previous ambiguity about the origin of the capacity for V_2O_5 in hydrated electrolytes represents the indispensable necessity of distinguishing between the genuine insertion of Mg^{2+} and various side reactions. Currently, new ideas and strategies are tested in sulfides or selenides as model compounds that are chemically stable in Mg^{2+} electrolytes, while oxides are awaiting proof or disproof of their inherent ability to intercalate Mg^{2+} in non-nucleophilic electrolytes. Alternatively, insertion cathodes based on conversion or displacement mechanisms are under initial development. Appreciating the history of the research on insertion cathodes for magnesium batteries, the present is a time for serious retrospect after a surge in preliminary and unverified results in the past. Such rigorous verification is essential to build a solid foundation for a genuine breakthrough in Mg^{2+} insertion cathodes for high energy, low cost rechargeable batteries.

Acknowledgement

H.D.Y. was supported by the National Research Foundation (NRF-2018R1C1B6004808 and NRF-2018R1A5A1025594) of the Korean Ministry of Science and ICT. S.H.O. acknowledges financial support from the KIST institutional program (Project No. 2E29641).

References

1. S. Jeong, D. Yoo, M. Ahn, P. Miró, T. Heine and J. Cheon, *Nat. Commun.*, 2015, **6**, 5763.
2. C. Wan, X. Gu, F. Dang, T. Itoh, Y. Wang, H. Sasaki, M. Kondo, K. Koga, K. Yabuki, G. J. Snyder, R. Yang and K. Koumoto, *Nat. Mater.*, 2015, **14**, 622.
3. A. V. Powell, *Annu. Rep. Prog. Chem., Sect. C: Phys. Chem.*, 1993, **90**, 177.
4. D. Aurbach, Z. Lu, A. Schechter, Y. Gofer, H. Gizbar, R. Turgeman, Y. Cohen, M. Moshkovich and E. Levi, *Nature*, 2000, **407**, 724.
5. D. Aurbach, G. S. Suresh, E. Levi, A. Mitelman, O. Mizrahi, O. Chusid and M. Brunelli, *Adv. Mater.*, 2007, **19**, 42607.
6. Y. Gu, Y. Katsura, T. Yoshino, H. Takagi and K. Taniguchi, *Sci. Rep.*, 2015, **5**, 12486.
7. X. Sun, P. Bonnick, V. Duffort, M. Liu, Z. Rong, K. A. Persson, G. Ceder and L. F. Nazar, *Energy Environ. Sci.*, 2016, **9**, 2273.
8. X. Sun, P. Bonnick and L. F. Nazar, *ACS Energy Lett.*, 2016, **1**, 297.
9. H. D. Yoo, Y. Liang, H. Dong, J. Lin, H. Wang, Y. Liu, L. Ma, T. Wu, Y. Li, Q. Ru, Y. Jing, Q. An, W. Zhou, J. Guo, J. Lu, S. T. Pantelides, X. Qian and Y. Yao, *Nat. Commun.*, 2017, **8**, 339.
10. N. Sa, H. Wang, D. L. Proffit, A. L. Lipson, B. Key, M. Liu, Z. Feng, T. T. Fister, Y. Ren, C.-J. Sun, J. T. Vaughey, P. A. Fenter, K. A. Persson and A. K. Burrell, *J. Power Sources*, 2016, **323**, 44.
11. S.-C. Lim, J. Lee, H. H. Kwak, J. W. Heo, M. S. Chae, D. Ahn, Y. H. Jang, H. Lee and S.-T. Hong, *Inorg. Chem.*, 2017, **56**, 7668.
12. R. Verrelli, A. P. Black, C. Pattanathummasid, D. S. Tchitchekova, A. Ponrouch, J. Oró-Solé, C. Frontera, F. Bardé, P. Rozier and M. R. Palacín, *J. Power Sources*, 2018, **407**, 162–172.
13. M. S. Whittingham, *Science*, 1976, **192**, 1126.
14. Y. Liang, H. D. Yoo, Y. Li, J. Shuai, H. A. Calderon, F. C. Robles Hernandez, L. C. Grabow and Y. Yao, *Nano Lett.*, 2015, **15**, 2194.
15. S. Jing, Y. Hyun Deog, L. Yanliang, L. Yifei, Y. Yan and C. G. Lars, *Mater. Res. Express*, 2016, **3**, 064001.
16. Z. Li, X. Mu, Z. Zhao-Karger, T. Diemant, R. J. Behm, C. Kübel and M. Fichtner, *Nat. Commun.*, 2018, **9**, 5115.
17. T. D. Gregory, R. J. Hoffman and R. C. Winterton, *J. Electrochem. Soc.*, 1990, **137**, 775.
18. P. G. Bruce, F. Krok, J. Nowinski, V. C. Gibson and K. Tavakkoli, *J. Mater. Chem.*, 1991, **1**, 705.
19. P. Novák and J. Desilvestro, *J. Electrochem. Soc.*, 1993, **140**, 140.
20. V. Shklover, T. Haibach, F. Ried, R. Nesper and P. Novák, *J. Solid State Chem.*, 1996, **123**, 317.
21. P. Novák, R. Imhof and O. Haas, *Electrochim. Acta*, 1999, **45**, 351.
22. G. G. Amatucci, F. Badway, A. Singhal, B. Beaudoin, G. Skandan, T. Bowmer, I. Plitz, N. Pereira, T. Chapman and R. Jaworski, *J. Electrochem. Soc.*, 2001, **148**, A940.

23. G. Gershinsky, H. D. Yoo, Y. Gofer and D. Aurbach, *Langmuir*, 2013, **29**, 10964.
24. R. E. Doe, C. M. Downie, C. Fischer, G. H. Lane, D. Morgan, J. Nevin, G. Ceder, K. A. Persson and D. Eaglesham, Pellion Technologies, Inc., *US Pat.*, US9240612B2, 2015.
25. T. S. Arthur, K. Kato, J. Germain, J. Guo, P.-A. Glans, Y.-S. Liu, D. Holmes, X. Fan and F. Mizuno, *Chem. Commun.*, 2015, **51**, 15657.
26. E. Levi, Y. Gofer and D. Aurbach, *Chem. Mater.*, 2010, **22**, 860.
27. S. Tepavcevic, Y. Liu, D. Zhou, B. Lai, J. Maser, X. Zuo, H. Chan, P. Král, C. S. Johnson, V. Stamenkovic, N. M. Markovic and T. Rajh, *ACS Nano*, 2015, **9**, 8194.
28. M. Rastgoo-Deylami, M. S. Chae and S.-T. Hong, *Chem. Mater.*, 2018, **30**, 7464.
29. D. B. Le, S. Passerini, F. Coustier, J. Guo, T. Soderstrom, B. B. Owens and W. H. Smyrl, *Chem. Mater.*, 1998, **10**, 682.
30. D. Imamura and M. Miyayama, *Solid State Ionics*, 2003, **161**, 173.
31. Q. Y. An, Y. F. Li, H. D. Yoo, S. Chen, Q. Ru, L. Q. Mai and Y. Yao, *Nano Energy*, 2015, **18**, 265.
32. A. Moretti and S. Passerini, *Adv. Energy Mater.*, 2016, **6**, 1600868.
33. J. T. Incorvati, L. F. Wan, B. Key, D. Zhou, C. Liao, L. Fuoco, M. Holland, H. Wang, D. Prendergast, K. R. Poeppelmeier and J. T. Vaughey, *Chem. Mater.*, 2016, **28**, 17.
34. L. F. Wan, J. T. Incorvati, K. R. Poeppelmeier and D. Prendergast, *Chem. Mater.*, 2016, **28**, 6900.
35. T. S. Arthur, N. Singh and M. Matsui, *Electrochem. Commun.*, 2012, **16**, 103.
36. N. Singh, T. S. Arthur, C. Ling, M. Matsui and F. Mizuno, *Chem. Commun.*, 2013, **49**, 149.
37. Y.-H. Tan, *et al.*, *ACS Nano*, 2018, **12**, 5856.
38. D. Pontiroli, *et al.*, *Carbon*, 2013, **51**, 143.
39. S. Margadonna, *et al.*, *J. Am. Chem. Soc.*, 2004, **126**, 15032.
40. D.-M. Kim, *et al.*, *Chem. Mater.*, 2018, **30**, 3199.
41. C. God, *et al.*, *RSC Adv.*, 2017, **7**, 14168.
42. P. Schoderböck and H. P. Boehm, *Synth. Met.*, 1991, **44**, 239.
43. T. Abe, N. Kawabata, Y. Mizutani, M. Inaba and Z. Ogumi, *J. Electrochem. Soc.*, 2003, **150**, A257.
44. H. Moon, *et al.*, *J. Phys. Chem. C*, 2014, **118**, 20246.
45. B. Jache and P. Adelhelm, *Angew. Chem., Int. Ed.*, 2014, **53**, 10169.
46. H. Kim, *et al.*, *Energy Environ. Sci.*, 2015, **8**, 2963.
47. M. R. Wagner, J. H. Albering, K.-C. Moeller, J. O. Besenhard and M. Winter, *Electrochem. Commun.*, 2005, **7**, 947.
48. H. Kuwata, M. Matsui and N. Imanishi, *J. Electrochem. Soc.*, 2017, **164**, A3229.
49. A. P. Cohn, *et al.*, *J. Mater. Chem. A*, 2016, **4**, 14954.
50. G. A. Elia, *et al.*, *J. Mater. Chem. A*, 2017, **5**, 9682.

51. M. Kawaguchi and A. Kurasaki, *Chem. Commun.*, 2012, **48**, 6897.
52. Y. Maeda and P. Touzain, *Electrochim. Acta*, 1988, **33**, 1493.
53. H. D. Yoo, *et al.*, *Nat. Commun.*, 2017, **8**, 339.
54. K. Goubitz, P. Capkova, K. Melanova, W. Molleman and H. Schenk, *Acta Crystallogr.*, 2001, **B57**, 178.
55. C. Wu, *et al.*, *Nat. Commun.*, 2013, **4**, 2431.
56. T. Nakato, Y. Furumi, N. Terao and T. Okuhara, *J. Mater. Chem.*, 2000, **10**, 737.
57. Y. Zhu, L. Peng, D. Chen and G. Yu, *Nano Lett.*, 2017, **16**, 742.
58. L. Peng, *et al.*, *Nano Lett.*, 2017, **17**, 6273.
59. G. He, W. H. Kan and A. Manthiram, *Chem. Mater.*, 2016, **28**, 682.
60. L. Zhou, *et al.*, *Adv. Mater.*, 2018, **30**, 1801984.
61. Y. Wang, *et al.*, *Adv. Mater.*, 2018, **30**, 1802563.
62. W. F. Hillebrand, *J. Am. Chem. Soc.*, 1907, **29**, 1019.
63. R. Allmann, I. Baumann, A. Kutoglu, H. Rösch and E. Hellner, *Die Naturwissenschaften*, 1964, **51**, 263.
64. S. Britto, *et al.*, *J. Am. Chem. Soc.*, 2015, **137**, 8499.
65. C. S. Rout, *et al.*, *J. Am. Chem. Soc.*, 2013, **135**, 8720.
66. X. Xu, *et al.*, *J. Mater. Chem. A*, 2014, **2**, 10847.
67. Y. L. Zhou, *et al.*, *ACS Appl. Mater. Interfaces*, 2016, **8**, 18797.
68. R. M. Sun, *et al.*, *ACS Appl. Mater. Interfaces*, 2015, **7**, 20902.
69. A. Kumar and S. M. Yusuf, *Phys. Rev. B*, 2005, **71**, 054414.
70. M. S. Chae, J. Hyoung, M. Jang, H. Lee and S.-T. Hong, *J. Power Sources*, 2017, **363**, 269.
71. X. Sun, V. Duffort and L. F. Nazar, *Adv. Sci.*, 2016, **3**, 1600044.
72. D. Asakura, *et al.*, *J. Am. Chem. Soc.*, 2013, **135**, 2793.
73. J. Song, *et al.*, *J. Am. Chem. Soc.*, 2015, **137**, 2658.
74. A. L. Lipson, *et al.*, *Chem. Mater.*, 2015, **27**, 8442.
75. R. Y. Wang, C. D. Wessells, R. A. Huggins and Y. Cui, *Nano Lett.*, 2013, **13**, 5748.
76. M. Pasta, C. D. Wessells, R. A. Huggins and Y. Cui, *Nat. Commun.*, 2012, **3**, 1149.
77. H.-W. Lee, *et al.*, *Nat. Commun.*, 2014, **5**, 5280.
78. L. Chen, *et al.*, *ACS Energy Lett.*, 2017, **2**, 1115.
79. H. D. Yoo, *et al.*, *Energy Environ. Sci.*, 2013, **6**, 2265.
80. M. Mao, T. Gao, S. Hou and C. Wang, *Chem. Soc. Rev.*, 2018, **47**, 8804.
81. P. Poizot, S. Laruelle, S. Grugeon, L. Dupont and J.-M. Tarascon, *Nature*, 2000, **407**, 496.
82. J. Cabana, L. Monconduit, D. Larcher and M. R. Palacin, *Adv. Mater.*, 2010, **22**, E170.
83. F. Klein, B. Jache, A. Bhide and P. Adelhelm, *Phys. Chem. Chem. Phys.*, 2013, **15**, 15876.
84. M. Armand and J.-M. Tarascon, *Nature*, 2008, **451**, 652.
85. P. G. Bruce, B. Scrosati and J.-M. Tarascon, *Angew. Chem., Int. Ed.*, 2008, **47**, 2930.

86. M. N. Obrovac, R. A. Dunlap, R. J. Sanderson and J. R. Dahn, *J. Electrochem. Soc.*, 2001, **148**, A576.
87. O. Crosnier and L. F. Nazar, *J. Electrochem. Soc.*, 2004, **7**, A187.
88. V. Duffort, X. Sun and L. F. Nazar, *Chem. Commun.*, 2016, **52**, 12458.
89. F. Xiong, *et al.*, *Nano Energy*, 2018, **47**, 210.
90. Y. Tashiro, K. Taniguchi and H. Miyasaka, *Chem. Lett.*, 2017, **46**, 1240.
91. Y. Tashiro, K. Taniguchi and H. Miyasaka, *Electrochim. Acta*, 2016, **210**, 655.
92. J. S. Chung and H. J. Sohn, *J. Power Sources*, 2002, **108**, 226.
93. C.-H. Lai, *et al.*, *J. Mater. Chem.*, 2010, **20**, 6638.
94. M.-Z. Xue, *et al.*, *J. Electrochem. Soc.*, 2006, **153**, A2262.
95. J.-L. Yue, Q. Sun and Z.-W. Fu, *Chem. Commun.*, 2013, **49**, 5868.